Journal of Materials Chemistry A

PAPER

View Article Online
View Journal | View Issue

Cite this: *J. Mater. Chem. A*, 2018, **6**, 24805

A highly robust and stable graphene-encapsulated Cu-grid hybrid transparent electrode demonstrating superior performance in organic solar cells†

Gyujeong Jeong,‡[a] Seungon Jung,‡[a] Yunseong Choi,[a] Junghyun Lee,[a] Jihyung Seo,[a] Dong Suk Kim*[b] and Hyesung Park*[a]

Received 13th October 2018
Accepted 19th November 2018

DOI: 10.1039/c8ta09868a

rsc.li/materials-a

Copper is one of the candidate materials for alternative transparent conductive electrodes (TCEs) owing to its excellent electrical conductivity and low cost. The vulnerability of copper against oxidation, however, imposes a severe limitation on its widespread application in functional devices. In this study, we demonstrate a high-performance and robust Cu and graphene hybrid TCE, where Cu optimized in a grid structure was used as the base electrode, while graphene sheet provided additional charge collection and transport pathways as well as a protective layer against oxidation of the underlying Cu. The Cu grid/graphene hybrid TCE was demonstrated in organic solar cells (OSCs) to have a power conversion efficiency of 8.5%, which is among the best performances based on metal grid TCE-based OSCs. The resulting device exhibited excellent long-term and thermal stabilities as well. The proposed Cu grid/graphene hybrid structure is expected to find practical application in various optoelectronics devices.

Introduction

Indium tin oxide (ITO) is commonly used as a transparent conductive electrode (TCE) owing to its low electrical conductivity and high optical transmittance. ITO has been widely adopted in various optoelectronic devices, including light-emitting diodes and solar cells.[1–4] However, several issues that are associated with ITO, such as chemical and mechanical weakness as well as scarcity of indium resources, continuously raise the demand for alternative TCEs.[5] In this regard, conducting polymers,[6,7] carbon nanotubes,[8–10] and graphene[11,12] have been investigated. Their chemical instability and insufficient electrical and optical properties, however, are still bottlenecks from a practical perspective.[13] On the other hand, metal-based materials with various architectures, including mesh type, nanowires, and nanofibers, show high conductivity and transmittance with large-area uniformity.[14,15] Most metal-based TCEs utilize noble metals such as gold or silver owing to their high conductivity despite the high cost.[16,17] Copper as an earth-abundant and cost-effective material exhibits decent electrical conductivity, *i.e.*, copper is about 10 000 and 100 times less expensive than gold and silver as well as approximately 45% more conductive than gold and only 5% less conductive than silver. However, the practical application of copper has been limited due to the oxidation issue. Several studies proposed the addition of protective layers on Cu nanostructures, such as noble metals (Ag, Au, Pt, *etc.*) or metal oxides.[18–20] However, additional issues arose, such as deteriorated transmittance or surface roughness in the composite structures. These challenges evidently impose severe limitations for developing high performance TCEs having widespread utilization.

Optical transmittance and electrical conductivity of metal grid-based TCEs are mostly governed by the trade-off between grid width and spacing. In particular, the void space in the grid can degrade the carrier collection efficiency in organic solar cells (OSCs).[21–25] An additional conducting medium is often used, such as a conducting polymer[26–29] or conducting oxide,[30,31] to form hybrid TCE structures for the improvement of the carrier collection efficiency of OSCs based on metal grid electrodes. Such hybrid structured electrodes, however, encounter additional issues, for instance, that conducting polymers or oxides can reduce the overall transparency as well as etch or oxidize the underlying metal grids.[32,33] These issues are detrimental for both device performance and stability. Graphene is considered as an attractive TCE material due to its high optical transparency, outstanding chemical stability, and good electrical properties.[34–36] Several studies have demonstrated the use

[a]*Department of Energy Engineering, School of Energy and Chemical Engineering, Low Dimensional Carbon Materials Center, Perovtronics Research Center, Ulsan National Institute of Science and Technology (UNIST), Ulsan 44919, Republic of Korea. E-mail: hspark@unist.ac.kr*

[b]*KIER-UNIST Advanced Center for Energy, Korea Institute of Energy Research (KIER), Ulsan 44919, South Korea. E-mail: kimds@kier.re.kr*

† Electronic supplementary information (ESI) available. See DOI: 10.1039/c8ta09868a

‡ These authors contributed equally to this work.

of graphene as a TCE in OSC applications either by itself[37–40] or by forming hybrid structures with metal meshes or nanowires.[41–43] For instance, Ag and Au grids with a graphene TCE were demonstrated in OSCs to have power conversion efficiencies (PCEs) of 3.80% and 4.38%, respectively.[41,42] In addition to the low efficiency, these studies used extra highly conducting polymers on the TCE for the operation of complete devices.

In this work, we present a metal grid/graphene hybrid TCE using earth-abundant and low-cost Cu and chemical vapor deposition (CVD) grown graphene. The graphene layer benefitted the charge collection efficiency and protected the underlying Cu. By optimizing the Cu grid geometry, this hybrid TCE exhibited excellent optical and electrical properties as well as robust chemical and thermal stabilities. The OSC based on this Cu grid/graphene TCE exhibited a PCE of 8.5%, which is among the highest values based on metal grid electrodes. Moreover, the hybrid electrode devices showed excellent long-term stability under various oxidizing conditions. These results suggest that Cu complemented with the graphene layer can function as an efficient and robust TCE platform that provides a promising alternative to ITO.

Experimental section

Fabrication of the Cu grid/graphene hybrid TCE

A Cu grid was fabricated using a conventional photolithography process and lift-off method. Cu was deposited onto the photoresist-patterned substrate by e-beam evaporation and the Cu grid pattern was obtained through the lift-off process by removing the photoresist. Graphene was synthesized on a 25 μm thick piece of copper foil *via* a low-pressure CVD method. The copper foil was loaded into the CVD chamber and ramped to 1000 °C for 30 min under hydrogen gas. After annealing at 1000 °C, graphene was grown by introducing methane gas. The as-synthesized graphene was transferred onto the Cu grid/substrate through a polymethylmethacrylate (PMMA)-assisted wet transfer method.

Fabrication of OSCs

OSCs were fabricated with the structure of glass/anode (ITO, Cu grid, or Cu grid/graphene)/hole transporting layer (HTL)/poly [[2,6′-4,8-di(5-ethylhexylthienyl)benzo[1,2-*b*;3,3-*b*]dithiophene] [3-fluoro-2[(2-ethylhexyl)carbonyl]thieno[3,4-*b*]thiophenediyl]] (PTB7-Th):[6,6]-phenyl C_{71}-butyric acid methyl ester ($PC_{71}BM$)/ZnO nanoparticle (NP)/Al. For Cu grid only OSCs, a conducting polymer (Clevios PH1000, Heraeus) was used as the HTL. Glass and ITO-coated glass substrates were cleaned in deionized water, acetone, and isopropyl alcohol by sonication, followed by O_2 plasma treatment. Poly(3,4-ethylenedioxythiophene):poly(styrene sulfonate) (PEDOT:PSS, Clevios AI4083, Heraeus) solution was spin-coated on ITO or Cu grid/graphene substrates at 4000 rpm for 1 min and subsequently annealed at 120 °C for 10 min. PTB7-Th and $PC_{71}BM$ were dissolved in chlorobenzene : 1,8-diiodooctane (97 : 3 vol%) with concentrations of 12 and 40 mg mL^{-1}, respectively. The blended solution was spin-coated at 900 rpm for 2 min onto the HTL. ZnO NP solution was spin-coated at 2000 rpm for 40 s. Finally, Al was thermally evaporated with a thickness of 100 nm under a base pressure of 2×10^{-6} Torr.

Measurements and characterization

Optical transmittance measurements were performed using a UV-vis-NIR spectrophotometer (Cary 5000, Agilent). The sheet resistance of the Cu grid/graphene electrode was obtained using the van der Pauw method (Keithley 2400 equipment). *J–V* characteristics were measured under AM 1.5G illumination using a xenon arc lamp solar simulator with a Keithley 2635A source meter. External quantum efficiency (EQE) measurements were performed with a QE system (QEX7, PV Measurements). Scanning electron microscopy (SEM, S-4800, Hitachi) and energy dispersive spectroscopy (EDS, S-4800, Hitachi) measurements were performed to analyze the surface morphology and elemental composition. A tapping mode atomic force microscope (AFM, DI-3100, Veeco) was used to analyze the surface morphology. X-ray photoelectron spectroscopy (XPS) spectra were obtained using an ESCALAB 250XI (Thermo Fisher Scientific). Neutral density filters were used to measure the light intensity dependence of J_{sc} and V_{oc}.

Results and discussion

The fabrication process of the Cu grid/graphene hybrid electrode is schematically illustrated in Scheme 1. The hexagonal structure of the Cu grid was prepared on target substrates *via* photolithography using a 60 nm Cu film deposited by e-beam evaporation. Graphene synthesized by the CVD process was transferred onto the Cu grid using PMMA as the supporting layer. The Cu grid/graphene hybrid electrode was treated in a vacuum for the conformal adhesion of graphene onto the Cu grid, after which PMMA was removed with acetone. Further details are provided in the Experimental section.

The electrical and optical properties of a Cu grid are closely related to its diagonal spacing (*D*) and width (*W*). Fig. 1a and b show the digital and optical microscopy (OM) images of Cu grids having various grid widths (3, 5, and 10 μm: denoted as D3, D5, and D10) and diagonal spacings (100, 200, and 300 μm: denoted as W100, W200, and W300), illustrating the dependency of the grid geometry on optical transparency and well-defined grid patterns. Fig. 1c presents the sheet resistance and transmittance at 550 nm of Cu grids with different widths and diagonal spacings. The sheet resistance of the Cu grid decreased with increasing grid width or decreasing grid diagonal spacing. In the case of Cu grids having a diagonal spacing of 100 μm, the sheet resistance was measured to be 6.02, 4.37, and 2.13 Ω sq^{-1} for W3, W5, and W10. For a grid width of 3 μm, the sheet resistance gradually increased from 6.02 to 9.78 and 10.8 Ω sq^{-1} for D100, D200, and D300, respectively. Similarly, the transmittance of the Cu grid electrode was also directly related to the geometry of the metal grid, *i.e.*, the transmittance increased with increasing grid spacing or decreasing grid width. To maximize the transmission of the incoming light, the grid width of the Cu grid electrode in this work was optimized to 3

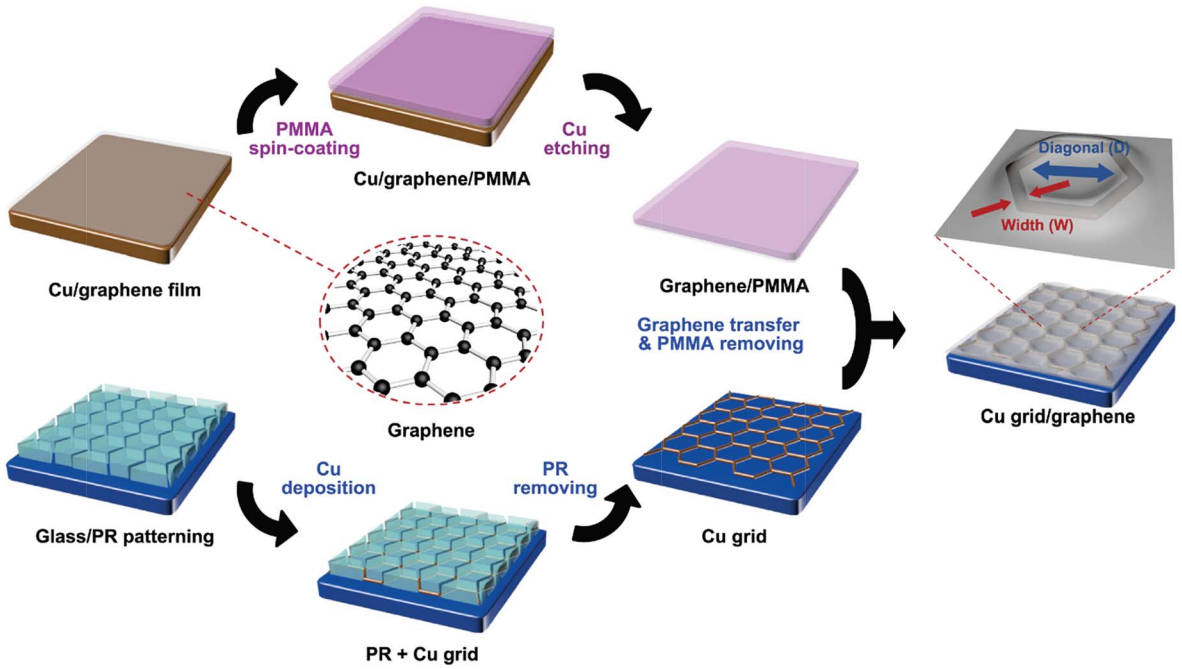

Scheme 1 Schematic for the fabrication process of the Cu grid/graphene hybrid TCE. The width and diagonal spacing of the Cu grid are indicated in the final Cu grid/graphene structure.

μm. The graphene that was transferred onto the Cu grid exhibited conformal coverage on the grid as shown in OM and SEM images (Fig. 1d). Fig. 1e shows the transmittance of the Cu grid (W3)/graphene having various diagonal spacings. The highest transmittance of 97.3% was obtained for D300W3. The decreased transmittance of 94.9% for the Cu grid (D300W3)/graphene hybrid compared with that of the pristine Cu grid (D300W3) is consistent with the absorption of monolayer graphene (~2.3%).[44] In comparison, a Cu thin film (5 nm) and ITO (150 nm) showed transmittances of 77.0% and 95.2% at 550 nm, respectively. We note that the optical transmittance of Cu grid/graphene exhibited high uniformity over a broad wavelength range of 350–800 nm compared with those of ITO and the Cu thin film, which is an advantage in optoelectronic device applications. In fact, the non-uniform optical transparency in thin metal films has been a challenging issue.[45,46] The sheet resistance of the hybrid film was also evaluated. The additional graphene layer improved the overall conductivity of the Cu grid by occupying the vacant spaces in the grid (Fig. 1f).[47] The aforementioned transmittance and sheet resistance data are summarized in Table S1 (ESI†).

The stability of the prepared Cu grid/graphene hybrid electrode was demonstrated under various environmental conditions. Fig. 2a shows the sheet resistance variations of the Cu grid and Cu grid/graphene that were exposed to ambient air at an elevated temperature of 240 °C and a relative humidity of 35–45%. The sheet resistance of the pristine Cu grid rapidly increased up to an exposure time of 30 min, after which it could not be measured any more due to severe oxidation.[48,49] The oxidized surface of Cu was clearly visualized from the OM image (Fig. 2b). In contrast, the sheet resistance and surface of the Cu grid/graphene hybrid electrode remained almost unchanged even after exposure under the same experimental conditions for 210 min. The stability of the Cu grid/graphene was also investigated under the acidic conditions of H_2SO_4 solution as shown in Fig. 2c. While the pristine Cu grid corroded rapidly and became completely insulating, the Cu grid/graphene retained its original electrical conductivity for a prolonged time duration. The etched surface of the Cu grid from the acidic solution is observed in Fig. 2d. In addition, the stability of the Cu grid/graphene was also investigated under basic conditions with 0.5 M sodium cholate solution as shown in Fig. S1 (ESI†). While the sheet resistance of the Cu grid electrodes showed a rapid increase under the basic conditions as well, the sheet resistance of the Cu grid/graphene electrodes exhibited negligible change under the same conditions. The stability analysis indicates that the TCEs based on the Cu grid/graphene hybrid are highly robust, and can withstand various processes involved in the fabrication of solar cells such as high temperature annealing or utilization of strong chemical solvents.

The thermal and chemical stabilities of the Cu grid/graphene were further investigated by chemical composition analysis, including XPS and EDS measurements. The samples were exposed to air at 240 °C and a relative humidity of 50% for 10 min. As shown in the XPS spectra of the Cu film in Fig. S2a (ESI†), a CuO peak appeared in the Cu 2p spectra and the intensity of the O peak in the O 1s spectra increased after the annealing. Such formation of CuO on the surface of Cu can cause the electrical conductivity to deteriorate. In contrast, both Cu 2p and O 1s spectra from the Cu film/graphene remained unchanged after the annealing. Thus, the graphene layer can function as an efficient protective layer against oxidation or

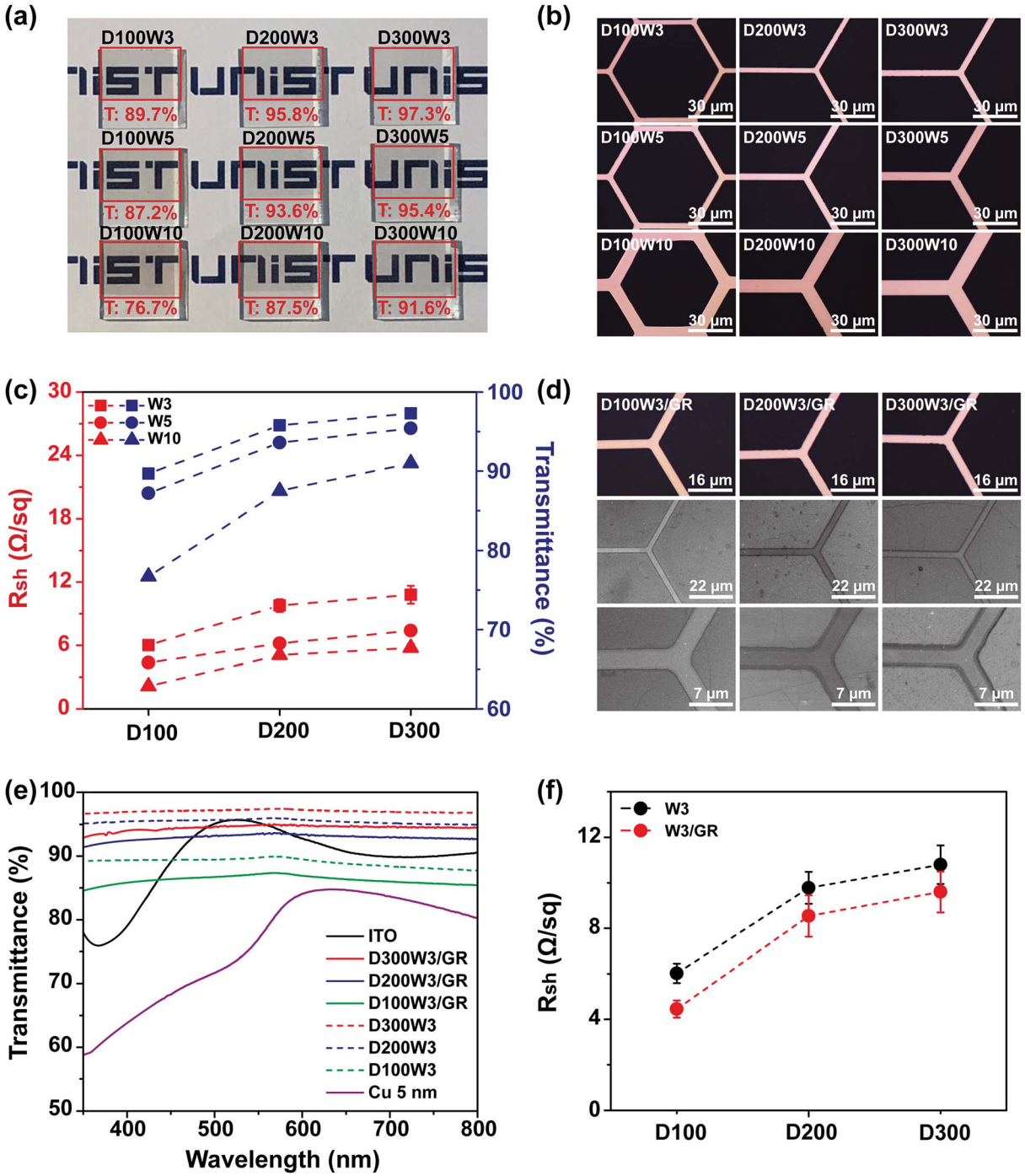

Fig. 1 Optical and electrical properties of the Cu grid and Cu grid/graphene. (a) Digital and (b) OM images of the Cu grid with various diagonal spacings and widths on glass substrates. (c) Sheet resistance and optical transmittance (at 550 nm) of the Cu grid having different diagonal spacings and widths. (d) OM (top) and SEM images of the Cu grid/graphene with different grid spacings. (e) Optical transmittance spectra of ITO, Cu thin film (5 nm), Cu grid, and Cu grid/graphene. (f) Sheet resistances of the Cu grid and Cu grid/graphene having varied grid spacings.

chemical reactions (Fig. S2b, ESI†). Fig. 2e–g show the SEM images and EDS elemental mapping of Cu and O from the Cu grid and Cu grid/graphene. The corresponding EDS spectra are provided in Fig. S3 (ESI†). Compared with the pristine Cu grid, the appearance of O element was clearly observed after its oxidation process. This oxidation effect was notably suppressed in the Cu grid/graphene hybrid. These results confirm that the graphene layer prevented the formation of the oxide layer on the Cu grid.

The Cu grid (W3)/graphene hybrid TCE was demonstrated in OSCs to have the structure of anode/PEDOT:PSS/PTB7-Th:$PC_{71}BM$/ZnO NP/Al (Fig. 3a). The corresponding flat-band energy level diagram is shown in Fig. 3b. The work function of the Cu grid/graphene measured by ultraviolet photoelectron

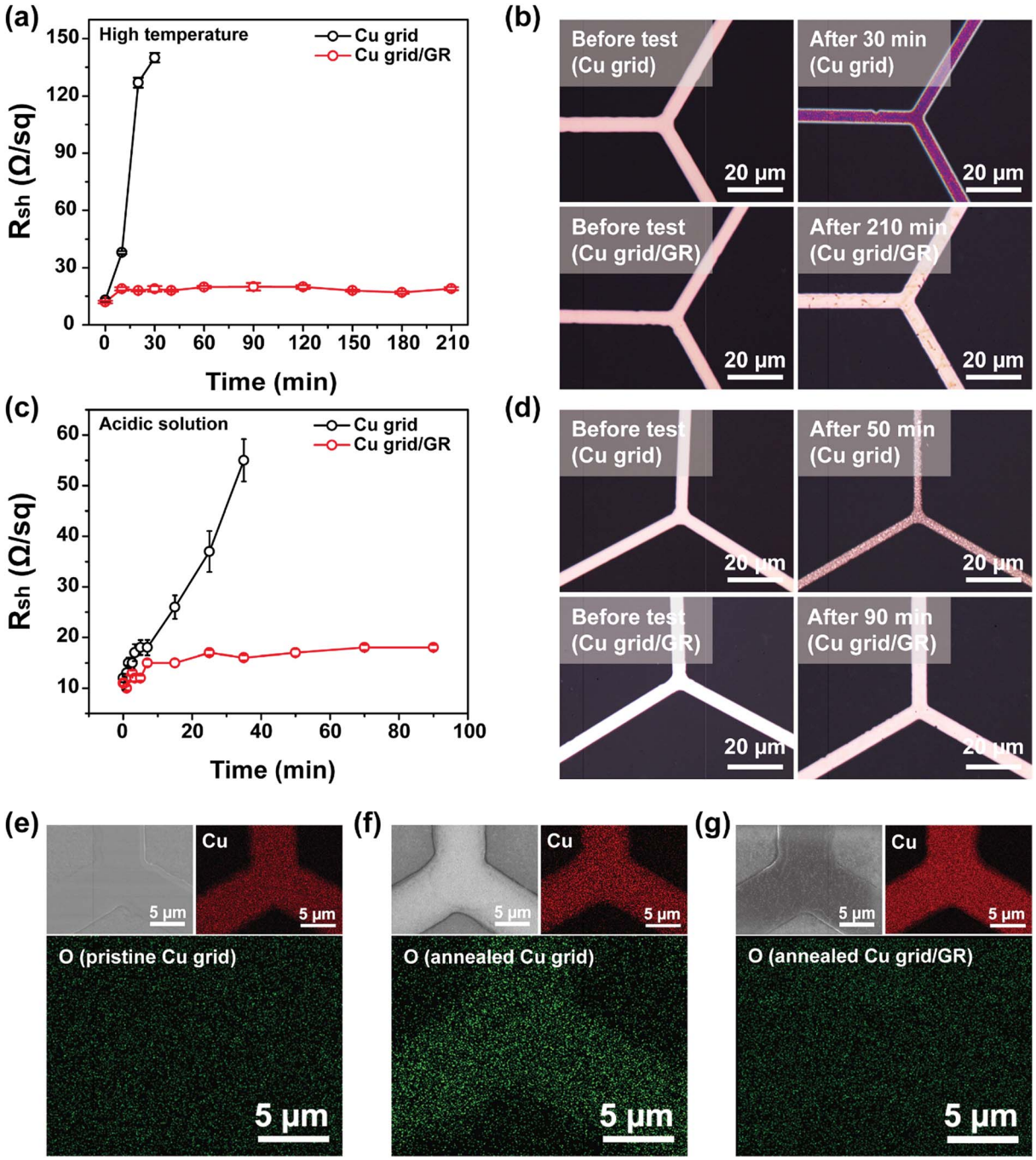

Fig. 2 Stability of the Cu grid and Cu grid/graphene. Change in sheet resistance of the pristine Cu grid and Cu grid/graphene exposed to (a) air at 240 °C and a relative humidity of 35–45% with the corresponding (b) OM images, and (c) acidic conditions of 0.5 M H_2SO_4 with the corresponding (d) OM images. SEM top-view images and EDS elemental mapping analysis (Cu and O) of (e) the pristine Cu grid as a reference, and (f) the Cu grid and (g) the Cu grid/graphene exposed to air at 240 °C for 10 min.

spectroscopy was 4.70 eV, which is comparable to that of ITO (Fig. S4, ESI†). The *J–V* characteristics were measured under simulated AM 1.5G standard illumination as shown in Fig. 3c, and the device performance parameters are summarized in Table 1. The Cu grid only devices exhibited negligible solar cell performances possibly due to the voids of grid spacings having poor charge collection.[23–25] The electrode based on the Cu grid/graphene hybrid having a diagonal spacing of 300 μm showed the best device performance with an open circuit voltage (V_{oc}) of 0.80 V, short circuit current density (J_{sc}) of 16.3 mA cm^{-2}, and fill factor (FF) of 65%, resulting in a PCE of 8.5%, making it slightly better than the ITO-based reference device having a PCE of 8.4%. A higher photocurrent was obtained in the device based on the Cu grid/graphene hybrid than the ITO-based reference device likely due to its better optical transmittance profile than that of ITO. These results indicate that the poor

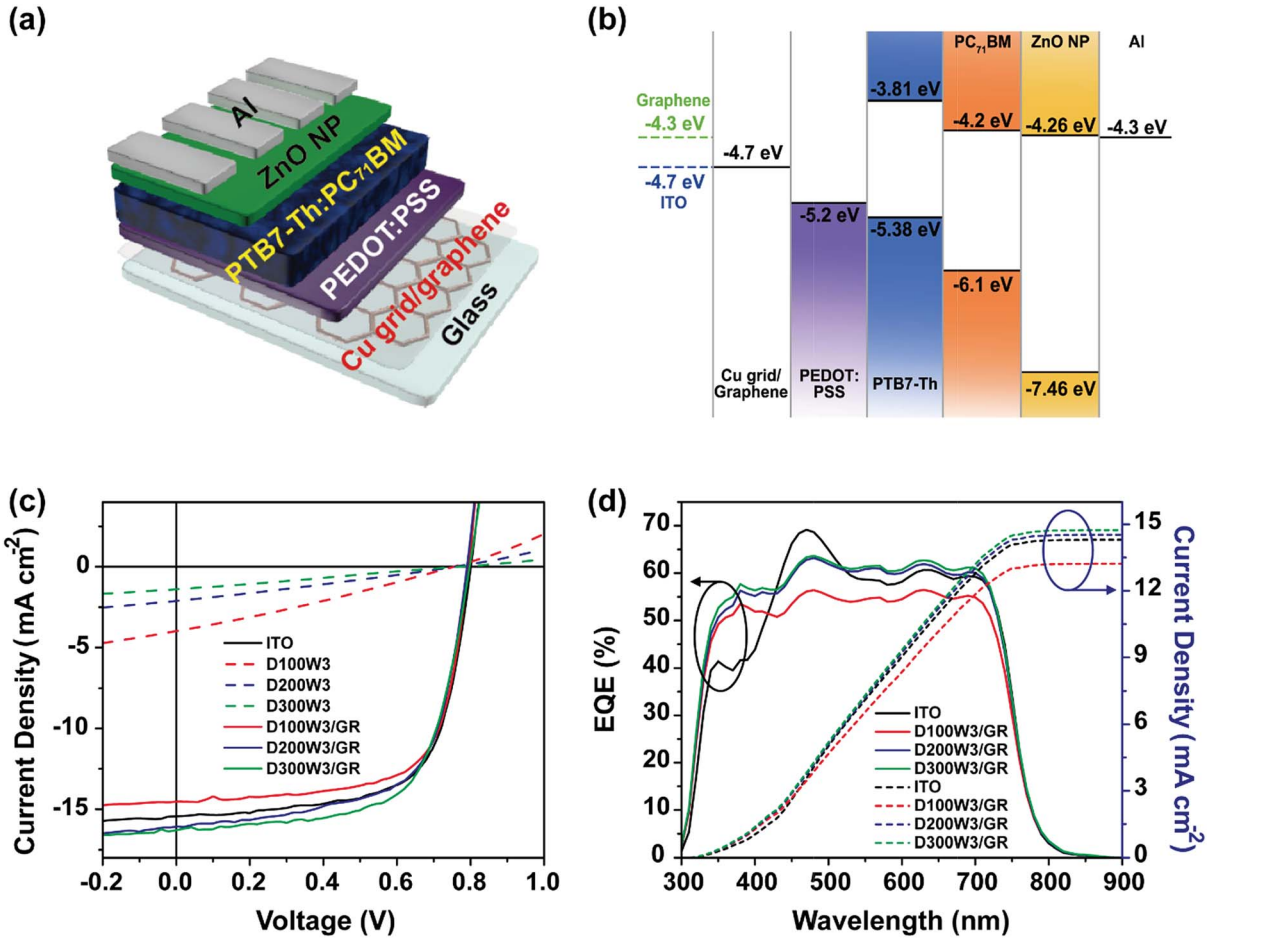

Fig. 3 Device performance of OSCs using Cu grid/graphene hybrid TCEs. (a) Schematic device structure of the Cu grid/graphene OSC and (b) the corresponding flat-band energy level diagram. (c) J–V characteristics of OSCs under AM 1.5G illumination at 100 mW cm^{-2}. (d) EQE spectra (solid line) and integrated photocurrent density (dashed line) of OSCs.

Table 1 Device performance parameters of PTB7-Th:$PC_{71}BM$-based OSCs using ITO, Cu grid, and Cu grid/graphene TCEs, respectively

Anode	J_{sc} [mA cm^{-2}]	V_{oc} [V]	FF [%]	PCE [%]
ITO	15.6	0.80	67	8.4 (8.2 ± 0.2)
Cu grid D100W3	4.0	0.75	28	0.8 (0.7 ± 0.1)
Cu grid D200W3	2.1	0.76	27	0.4 (0.4 ± 0.1)
Cu grid D300W3	1.4	0.77	26	0.3 (0.3 ± 0.1)
Cu grid D100W3/GR	14.5	0.79	69	7.9 (7.7 ± 0.1)
Cu grid D200W3/GR	16.1	0.79	65	8.2 (8.0 ± 0.2)
Cu grid D300W3/GR	16.3	0.80	65	8.5 (8.3 ± 0.3)

charge collection of empty spaces among Cu grids was successfully complemented by the graphene layer having good electrical conductivity and high charge carrier mobility. Fig. 3d presents the corresponding EQE measurements and the integrated photocurrent density results. The J_{sc} of the Cu grid/graphene (14.7 mA cm^{-2}) with a diagonal spacing of 300 μm obtained from the EQE measurement was slightly higher than that of ITO (14.3 mA cm^{-2}) due to the high and uniform optical transmittance in the full visible spectrum range. Compared with the previously reported OSCs based on transparent metal electrodes, the device performance in this work is among the best with a high optical transmittance of the TCE (Table S2, ESI†).

The charge carrier dynamics was investigated to evaluate the charge collection efficacy of the OSCs based on Cu grid/graphene electrodes. Fig. 4a and b show the recombination dynamics obtained from the light intensity (I) dependent J_{sc} and V_{oc} measurements, which was evaluated by analyzing the following relations: $J_{sc} \propto I^{\alpha}$ (where α is the coefficient of the power law) and the slope kT/q (where k, T, and q are Boltzmann's constant, absolute temperature, and elementary charge), respectively.[50,51] The higher α value of 0.98 and lower kT/q value of 1.62 for the Cu grid/graphene device than those of ITO indicate that the photogenerated charge carriers were effectively transported by mitigating the nongeminate recombination and Shockley–Read–Hall (trap-assisted) recombination. The smooth topography and full coverage of the PEDOT:PSS layer on the Cu grid/graphene electrode are important for minimizing potential leakage current generation in the completed devices. To confirm this, the Cu grid/graphene electrode after spin coating with PEDOT:PSS was analyzed by AFM. Fig. S5 (ESI†) shows that the PEDOT:PSS layer is conformally coated on the Cu grid/

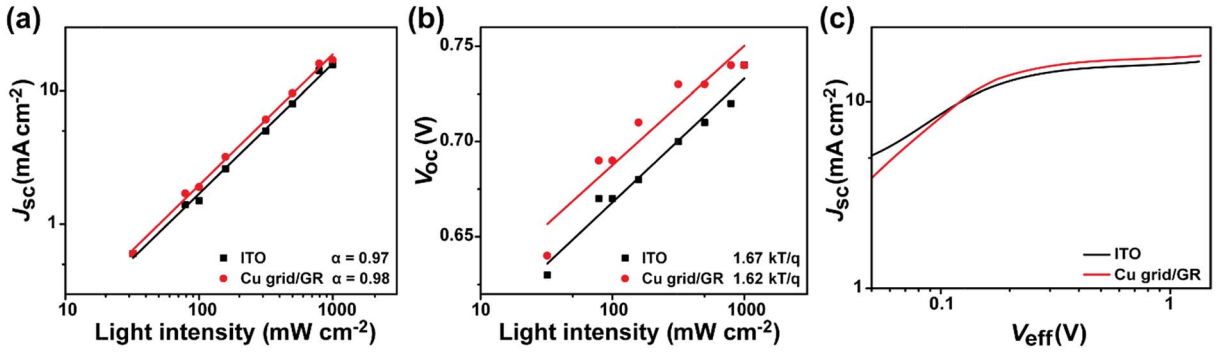

Fig. 4 Charge dynamics of OSCs having ITO and Cu grid/graphene TCEs. (a) J_{sc} and (b) V_{oc} plots depending on the light intensity. (c) Net photocurrent density *versus* effective voltage (J_{ph}–V_{eff}) of OSCs.

graphene electrode, which supports the idea that smoothening of the hybrid electrode can be achieved *via* full coverage by the PEDOT:PSS layer. Moreover, as revealed by the AFM measurements, the surface roughness of the Cu film was 1.4 ± 0.2 nm, which was further reduced to 1.1 ± 0.1 nm as the graphene layer was transferred onto the Cu film (Fig. S6, ESI†). This shows that graphene alleviates the roughness of the Cu film and would work efficiently by reducing the leakage current. High net photocurrent density (J_{ph}) was also observed in the device based on Cu grid/graphene electrodes as shown in Fig. 4c, and was evaluated using the following relation: $J_{ph} = J_L - J_D$. J_L and J_D are photocurrent densities under illumination and dark conditions, respectively. V_{eff} is defined as $V_{eff} = V_O - V_A$ (V_O is the voltage at which $J_{ph} = 0$ and V_A is the applied bias voltage). In addition, the maximum exciton generation rate, G_{max}, was calculated from the equation given by $J_{sat} = qG_{max}L$ (L is the thickness of the photoactive layer, 100 nm in our system),[52] and was 1.09×10^{28} and 1.02×10^{28} m^{-3} s^{-1} for devices with Cu grid/graphene and ITO, respectively. These results support the efficient charge collection capability in the Cu grid/graphene based OSCs.

To investigate the role of graphene in terms of stability in OSCs, we additionally prepared a hybrid electrode for comparison, which had highly conducting polymers of PEDOT:PSS (CLEVIOS PH 1000). The comparative device was fabricated with the structure of Cu grid (D300W3)/conducting polymer/PTB7-Th:$PC_{71}BM$/ZnO NP/Al. The resulting device efficiency was 8.0% as shown in Fig. S7 (ESI†). Fig. 5a shows the device stability results based on ITO, Cu grid/conducting polymer, and Cu grid/graphene electrodes, which were measured under inert conditions without encapsulation. Both ITO and Cu grid/graphene devices retained 98% of their initial efficiency even after 30 days. In contrast, the performance of the Cu grid/conducting polymer device rapidly dropped only after 3 days, which is possibly due to the damage in the Cu grid from the acidic and hygroscopic PEDOT:PSS. The device stability was also evaluated under ambient air conditions at room temperature. As shown in Fig. 5b, unlike the sharp decrease in PCE from the Cu grid/conducting polymer device, the Cu grid/graphene device exhibited much improved stability to the external environment and retained 40% of its initial performance after 170 hours. This stability is comparable to that of ITO-based devices. Furthermore, the thermal stability of the hybrid electrode was investigated by heating the completed devices from 30 to 150 °C under an inert environment for 10 min. Fig. 5c shows the device performance based on Cu grid/graphene and ITO electrodes, demonstrating that the hybrid electrode device was more thermally robust at elevated temperature ranges than the ITO sample. Such high performance of the Cu grid/graphene hybrid electrode provides a basis for its application in various optoelectronic devices as a promising alternative to ITO.

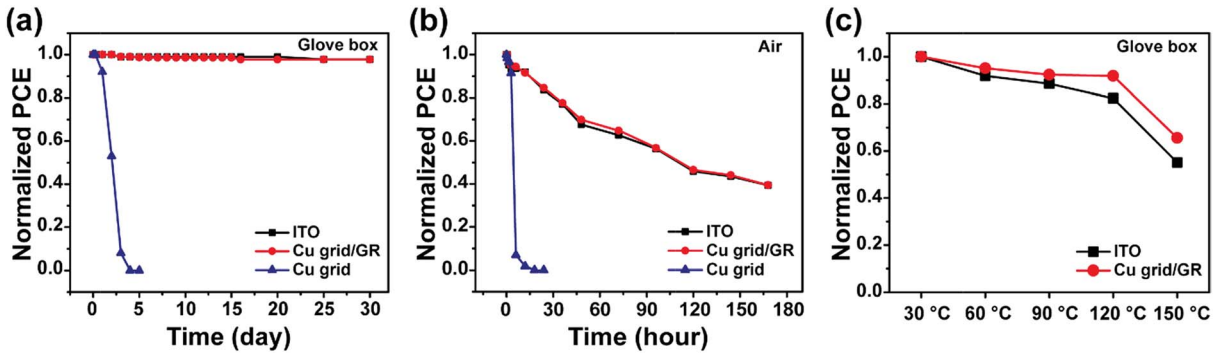

Fig. 5 Device stabilities of PTB7-Th:$PC_{71}BM$-based OSCs using ITO, Cu grid, and Cu grid/graphene TCEs exposed to various environments. Change in normalized PCE of OSCs (a) in a glovebox and (b) under ambient air conditions. (c) Thermal stability of the OSCs exposed to various temperatures under inert conditions. None of the tested devices were encapsulated.

Conclusions

In this work, a Cu grid and graphene hybrid TCE was successfully developed, and it demonstrated desirable optical transmittance, electrical conductivity, and chemical stability suitable for device applications. The monolayer graphene sheet not only provided good charge transport and collection pathways but also worked as an excellent protective layer to the underlying copper as well. The hybrid Cu grid/graphene film showed reliable durability even under harsh environments such as high temperature and highly humid and acidic conditions. The Cu grid/graphene electrode was utilized as the anode in OSCs. A PCE of 8.5% was achieved, which is one of the best performances among metal grid-based OSCs. Furthermore, the Cu grid/graphene-based OSCs demonstrated robust long-term operation stability under humid air and elevated temperature environments. These results demonstrate that the Cu grid/graphene hybrid structure as a promising alternative to ITO can contribute to the development of cost-effective and high-performance TCEs.

Conflicts of interest

There are no conflicts to declare.

Acknowledgements

G. J. and S. J. contributed equally to this work. This work was supported by the Basic Science Research Program through the National Research Foundation of Korea (NRF) funded by the Ministry of Education (2015R1D1A1A0105791) and Climate Change Program (NRF-2015M1A2A2056542). This study was also supported by the Development Program of the Korea Institute of Energy Research (KIER) (B8-2421) and the Research Project Funded by U-K Brand (1.180043.01) of UNIST (Ulsan National Institute of Science & Technology).

References

1 C. V. R. V. Kumar and A. Mansingh, *J. Appl. Phys.*, 1989, **65**, 1270–1280.
2 J. P. F. Lagerwall and G. Scalia, *Curr. Appl. Phys.*, 2012, **12**, 1387–1412.
3 S.-J. Su, T. Chiba, T. Takeda and J. Kido, *Adv. Mater.*, 2008, **20**, 2125–2130.
4 E. Bundgaard, F. Livi, O. Hagemann, J. E. Carlé, M. Helgesen, I. M. Heckler, N. K. Zawacka, D. Angmo, T. T. Larsen-Olsen, G. A. dos Reis Benatto, B. Roth, M. V. Madsen, M. R. Andersson, M. Jørgensen, R. R. Søndergaard and F. C. Krebs, *Adv. Energy Mater.*, 2015, **5**, 1402186.
5 D. S. Hecht, L. Hu and G. Irvin, *Adv. Mater.*, 2011, **23**, 1482–1513.
6 S. Kirchmeyer and K. Reuter, *J. Mater. Chem.*, 2005, **15**, 2077–2088.
7 A. A. Argun, A. Cirpan and J. R. Reynolds, *Adv. Mater.*, 2003, **15**, 1338–1341.
8 Z. C. Wu, Z. H. Chen, X. Du, J. M. Logan, J. Sippel, M. Nikolou, K. Kamaras, J. R. Reynolds, D. B. Tanner, A. F. Hebard and A. G. Rinzler, *Science*, 2004, **305**, 1273–1276.
9 M. Zhang, S. Fang, A. A. Zakhidov, S. B. Lee, A. E. Aliev, C. D. Williams, K. R. Atkinson and R. H. Baughman, *Science*, 2005, **309**, 1215–1219.
10 D. H. Zhang, K. Ryu, X. L. Liu, E. Polikarpov, J. Ly, M. E. Tompson and C. W. Zhou, *Nano Lett.*, 2006, **6**, 1880–1886.
11 K. S. Kim, Y. Zhao, H. Jang, S. Y. Lee, J. M. Kim, K. S. Kim, J. H. Ahn, P. Kim, J. Y. Choi and B. H. Hong, *Nature*, 2009, **457**, 706–710.
12 G. Eda, G. Fanchini and M. Chhowalla, *Nat. Nanotechnol.*, 2008, **3**, 270–274.
13 S. De and J. N. Coleman, *ACS Nano*, 2010, **4**, 2713–2720.
14 W.-K. Kim, S. Lee, D. H. Lee, I. H. Park, J. S. Bae, T. W. Lee, J.-Y. Kim, J. H. Park, Y. C. Cho, C. R. Cho and S.-Y. Jeong, *Sci. Rep.*, 2015, **5**, 10715.
15 K. Kim, J. Kim, B. G. Hyun, S. Ji, S.-Y. Kim, S. Kim, B. W. An and J.-U. Park, *Nanoscale*, 2015, **7**, 14577–14594.
16 C. J. Mulligan, M. Wilson, G. Bryant, B. Vaughan, X. Zhou, W. J. Belcher and P. C. Dastoor, *Sol. Energy Mater. Sol. Cells*, 2014, **120**, 9–17.
17 A. R. Rathmell, S. M. Bergin, Y.-L. Hua, Z.-Y. Li and B. J. Wiley, *Adv. Mater.*, 2010, **22**, 3558–3563.
18 I. E. Stewart, S. R. Ye, Z. F. Chen, P. F. Flowers and B. J. Wiley, *Chem. Mater.*, 2015, **27**, 7788–7794.
19 I. E. Stewart, A. R. Rathmell, L. Yan, S. Ye, P. F. Flowers, W. You and B. J. Wiley, *Nanoscale*, 2014, **6**, 5980–5988.
20 Z. Chen, S. Ye, I. E. Stewart and B. J. Wiley, *ACS Nano*, 2014, **8**, 9673–9679.
21 M. G. Kang, M. S. Kim, J. S. Kim and L. J. Guo, *Adv. Mater.*, 2008, **20**, 4408–4413.
22 J. Zou, H.-L. Yip, S. K. Hau and A. K. Y. Jen, *Appl. Phys. Lett.*, 2010, **96**, 203301.
23 P. Kuang, J.-M. Park, W. Leung, R. C. Mahadevapuram, K. S. Nalwa, T.-G. Kim, S. Chaudhary, K.-M. Ho and K. Constant, *Adv. Mater.*, 2011, **23**, 2469–2473.
24 H. M. Stec, R. J. Williams, T. S. Jones and R. A. Hatton, *Adv. Funct. Mater.*, 2011, **21**, 1709–1716.
25 H. Moon, H. Lee, J. Kwon, Y. D. Suh, D. K. Kim, I. Ha, J. Yeo, S. Hong and S. H. Ko, *Sci. Rep.*, 2017, **7**, 41981.
26 Y. Li, L. Mao, Y. Gao, P. Zhang, C. Li, C. Ma, Y. Tu, Z. Cui and L. Chen, *Sol. Energy Mater. Sol. Cells*, 2013, **113**, 85–89.
27 Y. H. Kim, L. Müller-Meskamp and K. Leo, *Adv. Energy Mater.*, 2015, **5**, 1401822.
28 J. Zou, H.-L. Yip, S. K. Hau and A. K. Y. Jen, *Appl. Phys. Lett.*, 2010, **96**, 203301.
29 J. Czolk, D. Landerer, M. Koppitz, D. Nass and A. Colsmann, *Adv. Mater. Technol.*, 2016, **1**, 1600184.
30 W. H. Zhang, J. Xiong, S. Wang, W. E. Liu, J. Li, D. F. Wang, H. S. Gu, X. B. Wang and J. H. Li, *J. Power Sources*, 2017, **337**, 118–124.
31 J.-A. Jeong, J. H. Kim and H.-K. Kim, *Sol. Energy Mater. Sol. Cells*, 2011, **95**, 1974–1978.
32 S. Chen, L. Song, Z. Tao, X. Shao, Y. Huang, Q. Cui and X. Guo, *Org. Electron.*, 2014, **15**, 3654–3659.

33 H.-G. Im, S. Jeong, J. Jin, J. Lee, D.-Y. Youn, W.-T. Koo, S.-B. Kang, H.-J. Kim, J. Jang, D. Lee, H.-K. Kim, I.-D. Kim, J.-Y. Lee and B.-S. Bae, *NPG Asia Mater.*, 2016, **8**, 282.
34 J. K. Wassei and R. B. Kaner, *Mater. Today*, 2010, **13**, 52–59.
35 C. Lee, X. D. Wei, J. W. Kysar and J. Hone, *Science*, 2008, **321**, 385–388.
36 X. Li, Y. Zhu, W. Cai, M. Borysiak, B. Han, D. Chen, R. D. Piner, L. Colombo and R. S. Ruoff, *Nano Lett.*, 2009, **9**, 4359–4363.
37 H. Park, Y. M. Shi and J. Kong, *Nanoscale*, 2013, **5**, 8934–8939.
38 S. Jung, J. Lee, J. Seo, U. Kim, Y. Choi and H. Park, *Nano Lett.*, 2018, **18**, 1337–1343.
39 H. Kim, J. Byun, S.-H. Bae, T. Ahmed, J.-X. Zhu, S.-J. Kwon, Y. Lee, S.-Y. Min, C. Wolf, H.-K. Seo, J.-H. Ahn and T.-W. Lee, *Adv. Energy Mater.*, 2016, **6**, 1600172.
40 H. Kim, S.-H. Bae, T.-H. Han, K.-G. Lim, J.-H. Ahn and T.-W. Lee, *Nanotechnology*, 2014, **25**, 014012.
41 M. J. Cha, S. M. Kim, S. J. Kang, J. H. Seo and B. Walker, *RSC Adv.*, 2015, **5**, 65646–65650.
42 J. H. Park, D. Y. Lee, Y. H. Kim, J. K. Kim, J. H. Lee, J. H. Park, T. W. Lee and J. H. Cho, *ACS Appl. Mater. Interfaces*, 2014, **6**, 12380–12387.
43 Y. Ahn, Y. Jeong, D. Lee and Y. Lee, *ACS Nano*, 2015, **9**, 3125–3133.
44 R. R. Nair, P. Blake, A. N. Grigorenko, K. S. Novoselov, T. J. Booth, T. Stauber, N. M. R. Peres and A. K. Geim, *Science*, 2008, **320**, 1308.
45 O. S. Hutter and R. A. Hatton, *Adv. Mater.*, 2015, **27**, 326–331.
46 G. Zhao, W. Wang, T. S. Bae, S. G. Lee, C. W. Mun, S. Lee, H. Yu, G. H. Lee, M. Song and J. Yun, *Nat. Commun.*, 2015, **6**, 8830.
47 M.-S. Lee, K. Lee, S.-Y. Kim, H. Lee, J. Park, K.-H. Choi, H.-K. Kim, D.-G. Kim, D.-Y. Lee, S. Nam and J.-U. Park, *Nano Lett.*, 2013, **13**, 2814–2821.
48 I. N. Kholmanov, S. H. Domingues, H. Chou, X. Wang, C. Tan, J.-Y. Kim, H. Li, R. Piner, A. J. G. Zarbin and R. S. Ruoff, *ACS Nano*, 2013, **7**, 1811–1816.
49 J. Song, J. Li, J. Xu and H. Zeng, *Nano Lett.*, 2014, **14**, 6298–6305.
50 S. R. Cowan, A. Roy and A. J. Heeger, *Phys. Rev. B: Condens. Matter Mater. Phys.*, 2010, **82**, 245207.
51 I. Riedel, J. Parisi, V. Dyakonov, L. Lutsen, D. Vanderzande and J.-C. Hummelen, *Adv. Funct. Mater.*, 2004, **14**, 38–44.
52 S. H. Liao, H. J. Jhuo, Y. S. Cheng and S. A. Chen, *Adv. Mater.*, 2013, **25**, 4766–4771.